

Second-order optical response of superconductors induced by supercurrent injection

Linghao Huang¹ and Jing Wang^{1,2,3,*}

¹State Key Laboratory of Surface Physics and Department of Physics, Fudan University, Shanghai 200433, China

²Institute for Nanoelectronic Devices and Quantum Computing, Fudan University, Shanghai 200433, China

³Zhangjiang Fudan International Innovation Center, Fudan University, Shanghai 201210, China

(Dated: October 3, 2023)

We develop a theory of the nonlinear optical responses in superconducting systems in the presence of a dc supercurrent. The optical transitions between particle-hole pair bands across the superconducting gap are allowed in clean superconductors as the inversion-symmetry-breaking by supercurrent. Vertex correction is included in optical conductivity to maintain the $U(1)$ gauge symmetry in the mean-field formalism, which contains the contributions from collective modes. We show two pronounced current dependent peaks in the second-order nonlinear optical conductivity $\sigma^{(2)}(\omega)$ at the gap edge $2\hbar\omega = 2\Delta$ and $\hbar\omega = 2\Delta$, which diverge in the clean limit. We demonstrate this in the models of single-band superconductor with s -wave and d -wave pairings, and Dirac fermion systems with s -wave pairing. Our theory predicts the current induced peak in $\text{Im}[\sigma^{(2)}(\omega)]$ is proportional to square of the supercurrent density in the s -wave single-band model, with the same order of magnitude as the recent experimental observation of second-harmonic generation in NbN by Nakamura *et al.* [*Phys. Rev. Lett.* **125**, 097004 (2020)]. The supercurrent induced nonlinear optical spectroscopy provides a valuable toolbox to explore novel superconductors.

I. INTRODUCTION

The linear and nonlinear optical spectroscopy methods are well established as a powerful experimental technique to explore quantum materials, in particular superconductors [1–4], which have long been in the focus of research. In semiconductors, the optical spectroscopy provides a direct and nondestructive measurements of pure spin currents [5–7]. In the context of superconductors, the linear optical measurements can unveil the characteristic nature of the superconducting state, for example, by probing spectral weight transfer [8] and measuring the superconducting gap size [9, 10], etc. Theoretically, the optical properties can be characterized by optical conductivity $\sigma(\omega)$, which can be calculated from microscopic considerations. The earliest analysis of the linear optical response for superconductors was made by Mattis and Bardeen in 1958 [11], who stated that in a single-band Bardeen-Cooper-Schrieffer (BCS) superconductor, the optical absorption (namely the real part of $\sigma^{(1)}(\omega)$) is absent when photon energy of incident light lies at or below the band gap in dirty limit (superconducting coherence length $\xi_0 \gg$ mean free path ℓ). Furthermore, optical transitions even vanishes at any finite frequency without the mediation of impurity [12], owing to the band structure of normal state: if the dispersion of electron satisfies $\epsilon_{\mathbf{k}} = \epsilon_{-\mathbf{k}}$, which can be guaranteed by inversion symmetry \mathcal{I} or time-reversal symmetry \mathcal{T} , when a Cooper pair is broken by light, the two electrons will have the same velocity but in opposite directions, resulting in zero net current. The Mattis-Bardeen theory, together with its generalization to arbitrary ℓ [13], has been tested very successful in explaining the linear optical properties of many superconductors. Recently, the

optical transitions in multi-band superconductor with \mathcal{I} symmetry were theoretically shown to be allowed, leading to new contribution to optical conductivity in clean limit ($\xi_0 \ll \ell$) [14].

Meanwhile the nonlinear response of superconductors attracts considerable interest. The second-order optical effects exist in superconductors with intrinsic broken \mathcal{I} symmetry of band structure or superconducting pairing order parameter [15–17]. The second-order nonlinear conductivity shows divergent behavior in low frequency limit, which is analogous to linear order case and unique to superconductors. Apart from quasiparticles, the excitation of collective modes in superconductors could also contribute to the optical response [18–23], where a well-known example is the third-harmonic generation of Higgs mode [24]. As a scalar excitation, Higgs mode can couple to gauge field at least in second order, giving rise to photocurrent with triple frequency of incident light. Therefore, the third-harmonic generation of superconductors would originate from both quasi-particle and Higgs mode excitation.

Recently, there is growing interest in the effect of supercurrent on optical response of superconductors. With the help of a dc supercurrent, Higgs mode can be excited linearly by electromagnetic field [25, 26], leading to linear optical response. Meanwhile, a dc supercurrent breaks \mathcal{I} symmetry extrinsically, thus makes $\epsilon_{\mathbf{k}} \neq \epsilon_{-\mathbf{k}}$, enabling nonzero optical response of clean single-band superconductors [27, 28]. Experimentally, optical response induced by supercurrent was measured in Nb₃Sn [29, 30] and NbN [31, 32] film, where the enhanced optical response near gap edge by supercurrent was observed in linear order optical effect, and the response peaks of second-harmonic generation (SHG) was detected.

It has been a longstanding proposal that gauge invariance should be maintained when calculating optical responses [33]. In the BCS mean-field formalism, the

* wjingphys@fudan.edu.cn

$U(1)$ gauge symmetry is broken, causing local charge non-conservation of optical response kernel and unphysical result in the longitudinal direction [34]. Nambu extended the vertex correction method widely used in quantum electrodynamics to resolve this issue [35], whose approach has been adopted in recent researches on the linear optical response of superconductor, and the vertex correction dramatically changes the linear optical conductivity [28, 36]. All of these previous studies focus on linear optical response, a natural question raises that how gauge invariance affects the nonlinear optical response of superconductors, which is the main theme of the current paper. We develop a theory of the nonlinear optical responses in clean superconducting systems in the presence of a dc supercurrent, with the vertex correction reflecting electron-electron interaction included. We show that the second-order optical conductivity $\sigma^{(2)}(\omega)$ depends on the nature of the normal state as well as the type of superconducting pairing, which is demonstrated in the model of single-band superconductor with s -wave and d -wave pairings, and Dirac fermion systems with s -wave pairing. Remarkably, we find the peak value of $\sigma^{(2)}(\omega)$ in s -wave superconductor have same order of magnitude as the SHG experimental measurement [32], which means the proposed effect here may very well already been observed. The supercurrent flow may be induced by an external magnetic field through the Meissner effect, thus the nonlinear optical spectroscopy provides a valuable toolbox to explore superconducting state.

The paper is organized as follows. Section II briefly review the diagrammatic method applied to superconductor in mean-field formalism. Section III present the formalism of gauge invariant second-order nonlinear optical response in superconductors by including vertex correction, which can be readily applied to higher-order responses. In Section IV, we calculate second-order nonlinear optical conductivity in several different superconductor models. Namely, the lattice model of single-band superconductor with s -wave and d -wave pairings, and Dirac fermion systems with proximity effect from s -wave superconductor. Finally, we conclude our work with some further discussions in Section V. Some auxiliary materials are relegated to Appendices.

II. DIAGRAMMATIC METHOD APPLIED TO SUPERCONDUCTOR

We start by briefly reviewing the mean-field theory of superconductor, specifically the diagrammatic method of the mean-field gap equation. The BCS mean field theory can be understood as the self-consistent Hartree-Fock (SCHF) approximation [35, 37]. To see this explicitly, we consider a two-dimensional system with an effective attracting two-body interaction between electrons. The interacting Hamiltonian is $H = \sum_{\mathbf{k}, \sigma} \epsilon_{\mathbf{k}} c_{\mathbf{k}, \sigma}^\dagger c_{\mathbf{k}, \sigma} - \sum_{\mathbf{k}, \mathbf{k}'} V_{\mathbf{k}, \mathbf{k}'} c_{\mathbf{k}, \uparrow}^\dagger c_{-\mathbf{k}, \downarrow}^\dagger c_{-\mathbf{k}', \downarrow} c_{\mathbf{k}', \uparrow}$. In the Nambu basis, the interaction term can be writ-

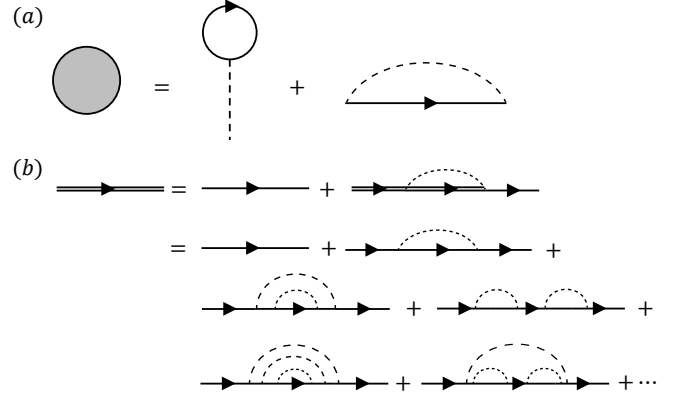


FIG. 1. (a) Feynman diagram of self-energy correction for electron Green's function up to first order. The first on right hand side represents Hartree term, and the second denotes Fock term. The single solid line represents electron Green's function, dashed line represents the electron-electron interaction. (b) Feynman diagram of Green's function corrected by interaction, which is represented by double solid line. Only off-diagonal correction is considered, and there is no crossing of interaction line.

ten as $\sum_{\mathbf{k}, \mathbf{k}'} V_{\mathbf{k}, \mathbf{k}'} [\Psi_{\mathbf{k}}^\dagger \tau_3 \Psi_{\mathbf{k}'}] [\Psi_{\mathbf{k}'}^\dagger \tau_3 \Psi_{\mathbf{k}}]$, where $\Psi_{\mathbf{k}} = (c_{\mathbf{k}, \uparrow}, c_{-\mathbf{k}, \downarrow}^\dagger)^T$ is the Nambu spinor operator, τ_3 is Pauli matrix. We approximate the four-fermion interaction by a quadratic term. Then, up to first order of interaction, the self-energy of electron can be written as,

$$\begin{aligned} \Sigma(k_0, \mathbf{k}) &= \Sigma_H + \Sigma_F(k_0, \mathbf{k}), \\ \Sigma_H &= -\frac{1}{\beta} \tau_3 \text{Tr} \left[\sum_{k'_0} \int \frac{d^2 \mathbf{k}'}{(2\pi)^2} V_{\mathbf{k}', \mathbf{k}} G(k'_0, \mathbf{k}') \tau_3 \right], \\ \Sigma_F(k_0, \mathbf{k}) &= \frac{1}{\beta} \sum_{k'_0} \int \frac{d^2 \mathbf{k}'}{(2\pi)^2} V_{\mathbf{k}-\mathbf{k}', \mathbf{k}} \tau_3 G(k_0 - k'_0, \mathbf{k} - \mathbf{k}') \tau_3, \end{aligned} \quad (1)$$

where $G(k_0, \mathbf{k}) = [ik_0 \tau_0 - H_0(\mathbf{k}) - \Sigma(k_0, \mathbf{k})]^{-1}$ is the Matsubara Green's function containing self-energy correction in Nambu basis, k_0 is the temporal component of the momentum, $H_0(\mathbf{k}) = \epsilon_{\mathbf{k}} \tau_3$ is the free Hamiltonian of the original band, and we have implied that $\epsilon_{\mathbf{k}} = \epsilon_{-\mathbf{k}}$. The corresponding Feynman diagrams of Hartree Σ_H and Fock $\Sigma_F(k_0, \mathbf{k})$ terms are shown in Fig. 1(a). Since the diagonal correction of self-energy only modifies the band structure and dose not contribute to pairing potential, we ignore this part, and define $\Sigma(k) = \Delta(k) \tau_1$. On this account, the Feynman diagram of corrected Green's function is constructed by adding interaction line that can transfer finite momentum, see Fig. 1(b). A typical character of this diagram is that no crossing of interaction line is considered. Therefore we retrieve the Bogoliubov-de Gennes (BdG) mean-field Hamiltonian from SCHF approximation as

$$H_{\text{BdG}} = \sum_{\mathbf{k}} \Psi_{\mathbf{k}}^\dagger \begin{pmatrix} \epsilon_{\mathbf{k}} & \Delta(\mathbf{k}) \\ \Delta(\mathbf{k}) & -\epsilon_{-\mathbf{k}} \end{pmatrix} \Psi_{\mathbf{k}}. \quad (2)$$

ity are defined as

$$\begin{aligned} j_a^{(1)} &= \sigma_{ab}^{(1)}(\omega) E_b(\omega), \\ j_a^{(2)} &= \sigma_{abc}^{(2)}(\omega_1 + \omega_2, \omega_1, \omega_2) E_b(\omega_1) E_c(\omega_2). \end{aligned} \quad (8)$$

$$\sigma_{ab}^{(1)}(\omega) = \frac{ie^2}{\hbar\omega} \frac{1}{\beta} \text{Tr} \sum_{k_0} \int \frac{d^2\mathbf{k}}{(2\pi)^2} [\gamma_{ab} G(k_0, \mathbf{k}) + \gamma_a G(k_0 + \omega_2, \mathbf{k}) \Gamma_b G(k_0, \mathbf{k})], \quad (9)$$

$$\begin{aligned} \sigma_{abc}^{(2)}(\omega_1 + \omega_2, \omega_1, \omega_2) &= \frac{e^3}{\hbar\omega_1\omega_2} \frac{1}{\beta} \text{Tr} \sum_{k_0} \int \frac{d^2\mathbf{k}}{(2\pi)^2} \left\{ \frac{1}{2} \gamma_{abc} G(k_0, \mathbf{k}) + \gamma_{ab} G(k_0 + \omega_2, \mathbf{k}) \Gamma_c G(k_0, \mathbf{k}) \right. \\ &\quad \left. + \frac{1}{2} \Gamma_a G(k_0 + \omega_1 + \omega_2, \mathbf{k}) \gamma_{bc} G(k_0, \mathbf{k}) + \Gamma_a G(k_0 + \omega_1 + \omega_2, \mathbf{k}) \Gamma_b G(k_0 + \omega_2, \mathbf{k}) \Gamma_c G(k_0, \mathbf{k}) + (b, \omega_1) \leftrightarrow (c, \omega_2) \right\}. \end{aligned} \quad (10)$$

Note that only the temporal component of photon momentum q is considered since spacial components \mathbf{q} are negligible small in terahertz region whose corresponding energy is comparable to the superconducting gap. The analytic continuation should be done in Green's function as $\omega \rightarrow \omega + i\eta$, where η is a infinitesimal positive parameter. Besides, we consider low temperature limit, i.e., the summation of Matsubara frequency can be replaced by integral. We study two processes in the second-order response: SHG and photocurrent effect (PC), characterized by $\sigma_{abc}^{(2)}(2\omega, \omega, \omega)$ and $\sigma_{abc}^{(2)}(0, \omega, -\omega)$, respectively. We will take both into account and show the frequency

The subscripts a, b, c are x or y in the two-dimensional system. After vertex correction, the gauge-invariant formulas for $\sigma_{ab}^{(1)}(\omega)$ and $\sigma_{abc}^{(2)}(\omega_1 + \omega_2, \omega_1, \omega_2)$ are given through Feynman diagrams shown in Fig. 3,

dependence of all the allowed components of them in the subsequent superconductor models.

IV. RESULTS FOR SUPERCONDUCTOR MODELS

Now we calculate second-order nonlinear optical conductivity $\sigma^{(2)}(\omega)$ in several different models of superconductors, which could exemplify the different aspects of supercurrent-enabled optical conductivity.

A. s -wave single-band superconductor

We first consider a single-band spin degenerate s -wave superconductor. A generic tight-binding model is on a square lattice with unit lattice constant, the nearest neighbor hopping t , the chemical potential μ and a superconducting gap Δ ,

$$H_{\text{TB}}^s(\mathbf{k}) = \begin{pmatrix} \epsilon_{\mathbf{k}+q\hat{x}} & \Delta \\ \Delta & -\epsilon_{-\mathbf{k}+q\hat{x}} \end{pmatrix}, \quad (11)$$

where $\epsilon_{\mathbf{k}} = t(2 - \cos k_x - \cos k_y) - \mu$. The model has C_{2x} symmetry when the supercurrent flows along the x direction. The symmetry allows two nonzero independent components of $\sigma^{(1)}$: $\sigma_{xx}^{(1)}, \sigma_{yy}^{(1)}$, and four possible nonzero independent components of $\sigma^{(2)}$: $\sigma_{xxx}^{(2)}, \sigma_{xyy}^{(2)}, \sigma_{yxy}^{(2)}, \sigma_{yyx}^{(2)}$. All of the rest components are zero. The intrinsic permutation symmetry leads to $\sigma_{abc}^{(2)}(\omega_1 + \omega_2, \omega_1, \omega_2) = \sigma_{acb}^{(2)}(\omega_1 + \omega_2, \omega_2, \omega_1)$, and reality condition requires $\sigma_{abc}^{(2)}(\omega_1 + \omega_2, \omega_1, \omega_2) = \left(\sigma_{abc}^{(2)}(-\omega_1 - \omega_2, -\omega_1, -\omega_2) \right)^*$. Thus we obtain the following relations of nonlinear optical responses in the low-frequency regime

$$\begin{aligned} \sigma_{abc}^{(2)}(2\omega, \omega, \omega) &= \sigma_{acb}^{(2)}(2\omega, \omega, \omega), \\ \sigma_{abc}^{(2)}(0, \omega, -\omega) &= \left(\sigma_{acb}^{(2)}(0, \omega, -\omega) \right)^*. \end{aligned} \quad (12)$$

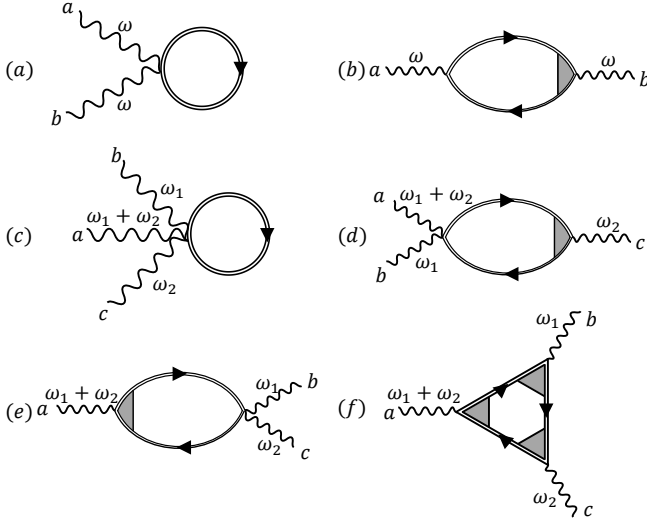


FIG. 3. (a), (b) Feynman diagrams contribute to first-order optical conductivity of superconductor. (c)-(f) Feynman diagrams contribute to second-order nonlinear optical conductivity of superconductor. Vertex correction under no-crossing approximation is considered. Note that to avoid double counting, no vertex correction in (a) and (c), and only one of the vertex is corrected in (b), (d) and (e).

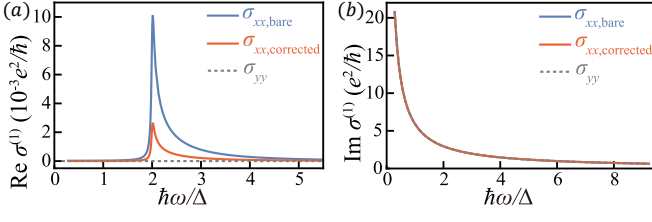


FIG. 4. $\sigma^{(1)}(\omega)$ of s -wave single-band model. (a) The real part of $\sigma_{xx}^{(1)}(\omega)$ without (blue solid line) and with (red solid line) vertex correction. (b) $\text{Im}[\sigma_{xx}^{(1)}(\omega)]$ without and with vertex correction. $\text{Im}[\sigma_{yy}^{(1)}(\omega)]$ (gray dashed line) is also shown.

Finally, only $\sigma_{xxx}^{(2)}, \sigma_{xyy}^{(2)}, \sigma_{yyx}^{(2)}$ are independent. In addition, $\sigma_{xxx}(0, \omega, -\omega)$ and $\sigma_{xyy}(0, \omega, -\omega)$ are real.

The numerical results of the linear, SHG and PC optical conductivity for the s -wave tight-binding model are shown in Fig. 4, Fig. 5, and Fig. 6, respectively. We set $t = 1 \times 10^2$ meV, $q_x = 0.02/a$, $a \sim 1$ Å is the lattice constant, $\mu = 0.9 \times 10^2$ meV, $V_{\mathbf{k}, \mathbf{k}'} = 1 \times 10^2$ meV, $\Delta \approx 4.5$ meV is determined by self-consistent gap equation, and $\eta = 10^{-1}$ meV. It is worth mentioning that the choice of the magnitude of momentum \mathbf{q} . The current density is defined as $\mathbf{J} = en_s \mathbf{v}_s$, where n_s is the superfluid density that can be determined by $\text{Im}[\sigma(\omega \rightarrow 0)] = \lim_{\omega \rightarrow 0} n_s e^2 / (m^* \omega)$. Therefore, $\mathbf{q} = m^* \mathbf{v}_s$ is estimated to be the order of $10^{-2}/a$ if the current injected into su-

perconductor is of about 1 A and the 2D superconducting film is 1 mm² in area.

For the linear optical conductivity $\sigma^{(1)}(\omega)$ shown in Fig. 4, its real part $\text{Re}[\sigma^{(1)}]$ is totally contributed from the bubble diagram in Fig. 3(b) owing to the purely imaginary of tadpole diagram in Fig. 3(a). Similar to the results of previous research [28], the real part shows a resonance peak near $\hbar\omega = 2\Delta$, which is caused by supercurrent, and has $1/\sqrt{\hbar\omega - 2\Delta}$ frequency dependence above gap edge. Below the gap edge, there is no optical transition, thus the real part vanishes. When vertex correction is included, the response is reduced in full frequency range. The imaginary part $\text{Im}[\sigma^{(1)}]$ is mainly contributed from the tadpole diagram, which has three order of magnitude larger than bubble diagram. $\text{Im}[\sigma^{(1)}(\omega)]$ has ω^{-1} frequency dependence as shown in Fig. 4(b), which reflects the Meissner effect. Meanwhile q has negligible effect on $\text{Im}[\sigma^{(1)}(\omega)]$. Since the dominant contribution comes from tadpole diagram, the vertex correction makes almost no difference and $\text{Im}[\sigma_{xx}^{(1)}(\omega)]$ is almost the same as $\text{Im}[\sigma_{yy}^{(1)}(\omega)]$.

For the second-order in Fig. 5 and Fig. 6, $\text{Im}[\sigma^{(2)}]$ vanishes below the superconducting gap, since no quasi-particle optical transition occurs, while $\text{Re}[\sigma^{(2)}] \propto \omega^{-2}$ in low-frequency limit. In the gapped s -wave superconductor with a dc supercurrent, both \mathcal{T} and \mathcal{I} symmetry are broken, but the combined of \mathcal{TI} symmetry is preserved, and the divergent behavior is attributed to the response of nonreciprocal superfluid density [16, 43]. Namely, the divergence of $\text{Re}[\sigma^{(2)}]$ is robust against the choice of $\mathbf{q} \neq 0$ and small parameter η in Green's function. In SHG of Fig. 5(b), there are two response peaks near $\hbar\omega = 2\Delta$ and $\hbar\omega = \Delta$ in $\text{Im}[\sigma_{\text{SHG}, xxx}^{(2)}]$, which are arising from bubble diagram in Fig. 3(d) and Fig. 3(e). The former has a peak near $\hbar\omega = 2\Delta$, and the latter has

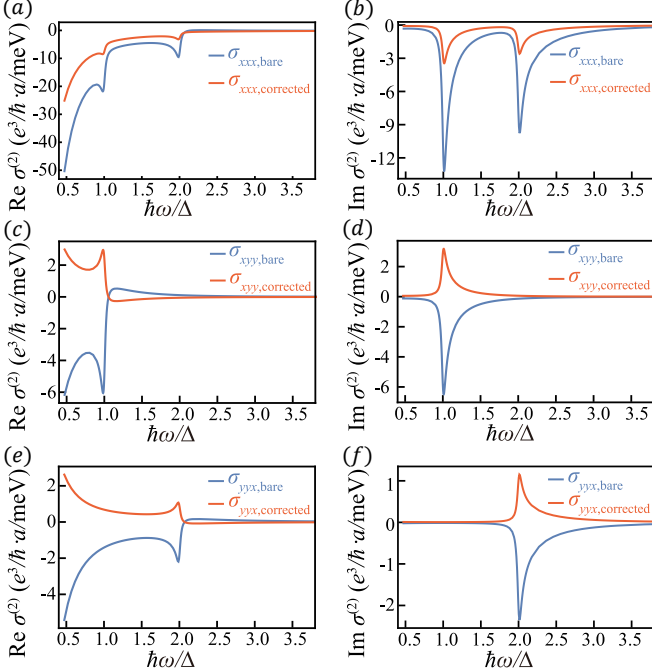


FIG. 5. $\sigma_{\text{SHG}}^{(2)}$ of s -wave single-band model. Blue and red lines show SHG without and with vertex correction, respectively. (a), (c), (e) are real part $\text{Re}[\sigma_{\text{SHG}}^{(2)}]$, (b), (d), (f) show imaginary part $\text{Im}[\sigma_{\text{SHG}}^{(2)}]$.

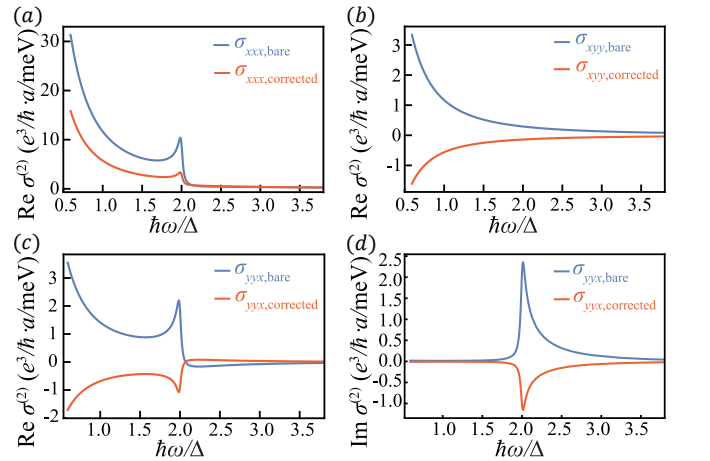


FIG. 6. $\sigma_{\text{PC}}^{(2)}$ of s -wave single-band model. Blue and red lines show PC without and with vertex correction, respectively. (a) $\text{Re}[\sigma_{\text{PC}, xxx}^{(2)}]$, (b) $\text{Re}[\sigma_{\text{PC}, xyy}^{(2)}]$, both of their imaginary parts are zero. (c) $\text{Re}[\sigma_{\text{PC}, yyx}^{(2)}]$. (d) $\text{Im}[\sigma_{\text{PC}, yyx}^{(2)}]$.

a peak near $\hbar\omega = \Delta$, which corresponds to and very well explained by the optical transition processes in Fig. 7(b) and Fig. 7(c), respectively. Remarkably, the current induced peak in $\text{Im}[\sigma_{\text{SHG},xxx}^{(2)}]$ at $\hbar\omega = 2\Delta$ is proportional to square of the supercurrent density, since it is mainly contributed from bubble diagram of Fig. 3(d). Since the bare vertex $\gamma_{xy} = 0$, Fig. 3(d) does not contribute to $\sigma_{\text{SHG},xyy}^{(2)}$, thus there is no peak near $\hbar\omega = 2\Delta$. Similarly, $\sigma_{\text{SHG},yyx}^{(2)}$ does not show the peak near $\hbar\omega = \Delta$ due to $\gamma_{yx} = 0$ and no contribution from Fig. 3(e). Meanwhile, in Fig. 6 for PC, only the resonant peak near $\hbar\omega = 2\Delta$ may exist, as seen in $\sigma_{\text{PC},xxx}^{(2)}$ and $\sigma_{\text{PC},yyx}^{(2)}$. No peak will appear near $\hbar\omega = 2\Delta$ in $\sigma_{\text{PC},xyy}^{(2)}$ for $\gamma_{xy} = 0$. For both SHG and PC processes in the second-order response, the asymptotic behavior near $\hbar\omega = \Delta$ has similar form to that near $\hbar\omega = 2\Delta$. Namely, the frequency dependence of $\text{Re}[\sigma^{(2)}]$ shows $1/\sqrt{\Delta - \hbar\omega}$ and $1/\sqrt{2\Delta - \hbar\omega}$ when $\hbar\omega$ is below Δ and 2Δ , respectively. While $\text{Im}[\sigma^{(2)}]$ scales as $1/\sqrt{\hbar\omega - \Delta}$ and $1/\sqrt{\hbar\omega - 2\Delta}$ above the resonance frequencies. After vertex correction, all the magnitude of second-order response is reduced, $\sigma_{xyy}^{(2)}$ and $\sigma_{yyx}^{(2)}$ even reverse sign, while the shape of frequency dependence curve is unchanged. Interestingly, we find that in this model, the contribution from triangular diagram of Fig. 3(f) can be neglected compared with tadpole (Fig. 3(c)) and bubble (Fig. 3(d) and 3(e)) diagrams, where the latter reveals similar resonant behaviors and asymptotic frequency dependence to that of linear order.

B. Dirac fermion with s -wave pairing

Then we proceed to study the Dirac fermion with an s -wave superconducting pairing, which describes the surface state of a 3D topological insulator with the proximity effect from a conventional s -wave superconductor [44]. In the presence of a dc supercurrent, the BdG Hamiltonian is

$$H_{\text{BdG}}^{\text{Dirac}}(\mathbf{k}) = (\hbar v(k_x + q_x)s_y - \hbar v k_y s_x - \mu)\tau_z + \Delta\tau_x. \quad (13)$$

Here v is the Fermi velocity, we set μ staying high above Dirac point. Thus we can focus on the upper Dirac bands around the proximity gap when the photon is in the terahertz frequency. The projected single-band model for Dirac fermion is

$$H_{\text{BdG}}^{\text{D}}(\mathbf{k}) = \hbar v q_x \hat{k}_x \tau_0 + (\hbar v k - \mu)\tau_z + \Delta\tau_x. \quad (14)$$

where $\hat{k}_x \equiv k_x/k$, and $k = \sqrt{k_x^2 + k_y^2}$. The model has C_{2x} symmetry, similar to the above s -wave single-band model, the symmetry allowed nonzero independent components are $\sigma_{xx}^{(1)}, \sigma_{yy}^{(1)}$ for linear order, and $\sigma_{xxx}^{(2)}, \sigma_{xyy}^{(2)}, \sigma_{yyx}^{(2)}$ for second order.

The numerical results of linear, SHG and PC optical conductivity for Dirac fermion model are shown in Fig. 8

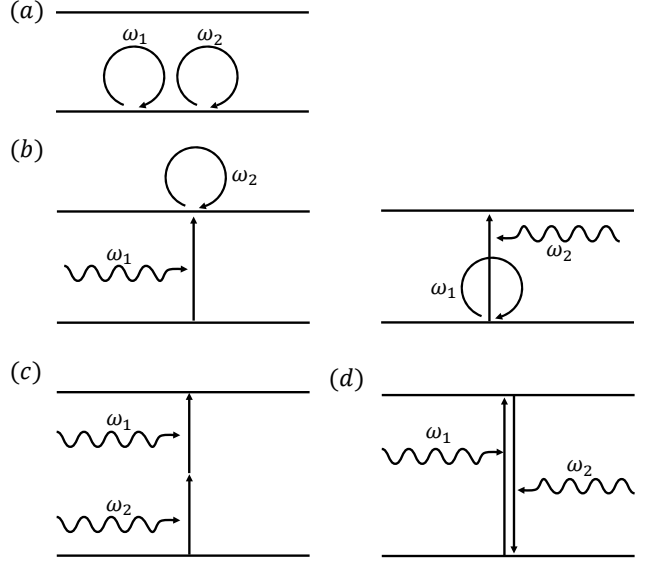


FIG. 7. Schematic picture for the second-order optical process. (a) Pure intraband response, and no resonant frequency appears. (b) Interband and intraband mixing process. In SHG and PC, resonance happens at $\hbar\omega = 2\Delta$. (c), (d) Pure interband process. At $\hbar\omega = \Delta$, resonance occurs in SHG (c), while no resonance appears in PC (d).

and Fig. 9, respectively. Meanwhile, for comparison, the analytic results for the responses without vertex correction are listed in Appendix C. We set $q_x = 0.005/a$, $\mu = 2 \times 10^2$ meV, $V_{\mathbf{k},\mathbf{k}'} = 0.8 \times 10^2$ meV, $\hbar v a = 6.6 \times 10^2$ meV, $\eta = 5 \times 10^{-2}$ meV, then $\Delta \approx 5$ meV. Due to the linear dispersion of Dirac fermion, all vertex functions with more than one-photon are zero. As a result, only bubble diagram (Fig. 3(b)) contributes to $\sigma^{(1)}$ and triangular diagram (Fig. 3(f)) contributes to $\sigma^{(2)}$. As shown in Fig. 8 and Fig. 9, in low frequency regime, $\text{Im}[\sigma^{(1)}]$ shows ω^{-1} behavior and $\text{Re}[\sigma^{(2)}]$ has ω^{-2} behavior. Below the superconducting gap, there is no optical transition, $\text{Re}[\sigma^{(1)}]$ and $\text{Im}[\sigma^{(2)}]$ vanish. Without vertex correction, $\text{Re}[\sigma^{(1)}]$ has $1/\sqrt{\hbar\omega - 2\Delta}$ asymptotic behaviors above gap edge, and $\text{Im}[\sigma^{(1)}]$ scales as $1/\sqrt{2\Delta - \hbar\omega}$ below gap edge [Fig. 8 red dash], which are the feature from

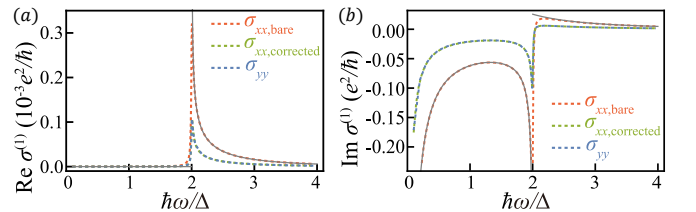


FIG. 8. $\sigma^{(1)}(\omega)$ of Dirac fermion model. Red (green) dashed line denotes $\sigma_{xx}^{(1)}(\omega)$ without (with) vertex correction, $\sigma_{yy}^{(1)}(\omega)$ is shown in blue. (a) $\text{Re}[\sigma^{(1)}]$. (b) $\text{Im}[\sigma^{(1)}]$. Gray lines are the analytical results of $\sigma^{(1)}(\omega)$ without vertex correction in Appendix C.

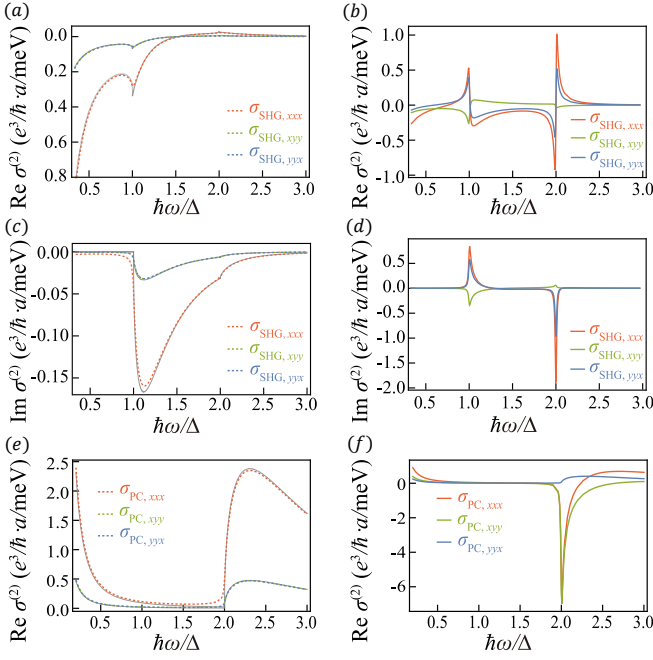


FIG. 9. $\sigma^{(2)}$ of Dirac fermion model. (a) and (c) are real and imaginary part of σ_{SHG} without vertex correction, Gray lines are the analytical result without vertex correction. (e) is real part of σ_{PC} without vertex correction. The optical spectrum of σ_{xyy} and σ_{yyx} are the same. Corresponding results with vertex correction are shown in (b), (d) and (f), respectively. After vertex correction, σ_{xyy} and σ_{yyx} differ.

bubble diagram. While for $\sigma^{(2)}$, no sharp peak appears as shown in Fig. 9(a), 9(c) and 9(e), which is the feature of triangular diagram. When vertex correction is considered, the real and imaginary parts of $\sigma^{(1)}$ are reduced since both of them are purely contributed from bubble diagram. However, the vertex correction does not change the resonance shape of response curve in $\sigma^{(1)}$. In addition, the vertex corrected $\sigma_{xx}^{(1)}$ is identical to $\sigma_{yy}^{(1)}$, which is consistent with previous research [27]. While in the second order response, besides the quantitative difference between bare value and vertex corrected $\sigma^{(2)}$, the sharp peaks appear near $\hbar\omega = \Delta$ and $\hbar\omega = 2\Delta$ with vertex correction.

C. d -wave single-band superconductor

Finally, we study different type of superconducting pairing, namely a single-band spin degenerate d -wave superconductor. The tight-binding model on a square lattice is

$$H_{\text{TB}}^d(\mathbf{k}) = \begin{pmatrix} \epsilon_{\mathbf{k}+q\hat{x}} & \Delta\phi_{\mathbf{k}} \\ \Delta\phi_{\mathbf{k}} & -\epsilon_{-\mathbf{k}+q\hat{x}} \end{pmatrix}, \quad (15)$$

where $\epsilon_{\mathbf{k}} = t(2 - \cos k_x - \cos k_y - \mu)$, $\phi_{\mathbf{k}} = (\cos k_x - \cos k_y)$. The independent nonzero components of $\sigma^{(1)}$ and $\sigma^{(2)}$ are

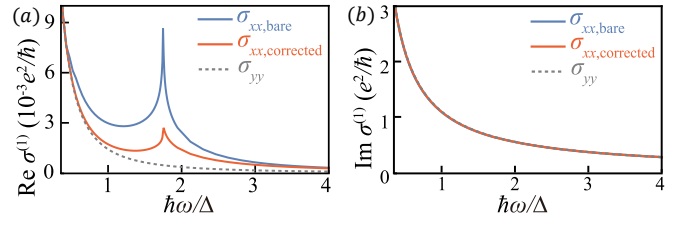


FIG. 10. $\sigma^{(1)}(\omega)$ of d -wave single-band model. (a) $\text{Re}[\sigma_{xx}^{(1)}(\omega)]$ without (blue solid line) and with (red solid line) vertex correction. (b) $\text{Im}[\sigma_{xx}^{(1)}(\omega)]$ without and with vertex correction. $\sigma_{yy}^{(1)}(\omega)$ (gray dashed line) is also shown.

the same as in the s -wave model, since the d -wave model here has C_{2x} symmetry with the supercurrent flows along x axis. In the numerical calculations for $\sigma^{(1)}$ and $\sigma^{(2)}$, we set $q_x = 0.07/a$, $\mu = 0.9 \times 10^2$ meV, $V = 1.8 \times 10^2$ meV, $\eta = 3 \times 10^{-2}$ meV, and $\Delta \approx 23$ meV determined by Eq. (3).

Due to the nodal character of quasiparticle spectrum, when a supercurrent is induced inside a d -wave superconductor, there exists a Bogoliubov Fermi surface which causes intraband conductivity. To capitalize the intraband response, we replace the factor $1/\omega$ in Eq. (9) and $1/(\omega_1\omega_2)$ in Eq. (10) by $1/(\omega + i\eta')$ and $1/(\omega_1 + i\eta')(\omega_2 + i\eta')$, respectively [45]. This corresponding to adiabatic switching the electrodynamic field

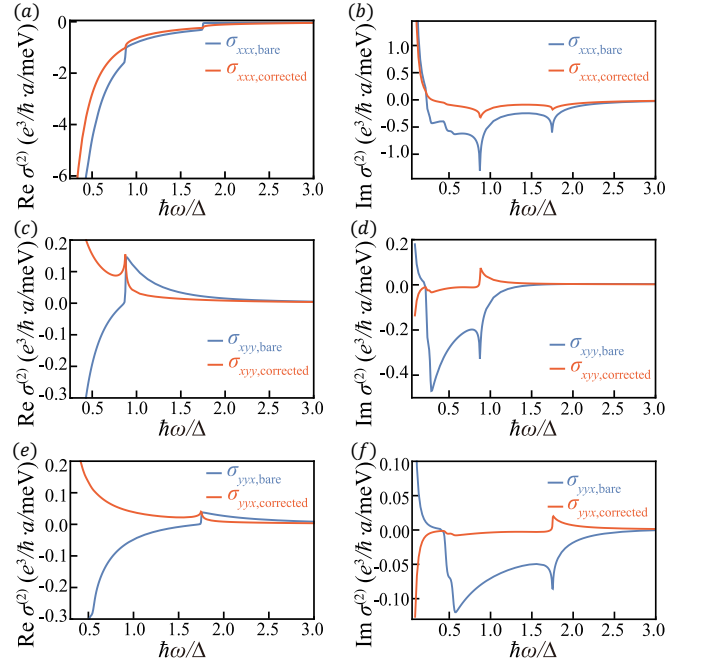


FIG. 11. $\sigma_{\text{SHG}}^{(2)}$ of d -wave single-band model. Blue and red lines show σ_{SHG} without and with vertex correction, respectively. (a), (c), (e) are real part $\text{Re}[\sigma_{\text{SHG}}^{(2)}]$, (b), (d), (f) show imaginary part $\text{Im}[\sigma_{\text{SHG}}^{(2)}]$

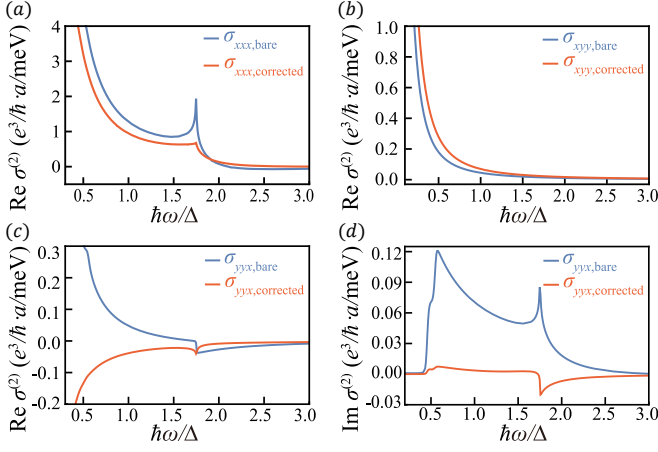


FIG. 12. $\sigma_{PC}^{(2)}$ of d -wave single-band model. Blue and red lines show PC without and with vertex correction, respectively. (a) $\text{Re}[\sigma_{PC,xxx}^{(2)}]$, (b) $\text{Re}[\sigma_{PC,xyy}^{(2)}]$, both of their imaginary parts are zero. (c) $\text{Re}[\sigma_{PC,yyx}^{(2)}]$. (d) $\text{Im}[\sigma_{PC,yyx}^{(2)}]$.

as $\mathbf{A}(t)e^{-\eta't}$, here we choose $\eta' = \eta$. Fig. 10 shows the linear optical conductivity with and without vertex correction. Near $\hbar\omega = 2\Delta$, a peak induced by supercurrent appears in $\text{Re}[\sigma_{xx}^{(1)}]$, which is reduced when considering the vertex correction as expected. The intraband response gives a Drude peak in low frequency regime and scales as $\eta'/(\eta'^2 + \omega^2)$. As the same as s -wave superconductor, the dominant contribution to $\text{Im}[\sigma^{(1)}]$ comes from the tadpole diagram that accounts for the Meissner effect.

Fig. 11 and Fig. 12 show second-order processes SHG and PC, respectively. The real part of σ_{SHG} and σ_{PC} show ω^{-2} divergent behavior. While the imaginary part $\text{Im}[\sigma^{(2)}]$ has a finite contribution from intraband response in low frequency region, which is different from s -wave case where $\text{Im}(\sigma^{(2)})$ vanishes due to the superconducting gap. Therefore, the current-induced second-order optical effect could distinguish different superconducting order parameters. Also different from s -wave case, there are some kinks in $\text{Im}[\sigma^{(2)}]$ of d -wave superconductor when $\hbar\omega/2\Delta \sim 0.5$ (i.e. $\hbar\omega \sim 10$ meV), which corresponds to the optical transition happens near the Bogoliubov Fermi surface, and may come from Van Hove singularities. In general, the vertex correction will reduce the magnitude of second-order response and some components even reverse sign, while with one exception $\sigma_{PC,xyy}^{(2)}$ gets enhanced.

V. DISCUSSION

We compare the magnitude of the predicted effect to the present experiments on second-order optical conductivity of superconductors. A current enabled SHG was recently reported in the experimental of Ref. [32]. In that experiment, the observed SHG nonlinear susceptibility

attributed to the supercurrent flow in the NbN superconductor thin film can reach $\chi_{ex}^{(2)} \sim 2.2 \times 10^8$ pm/V near the resonance frequency $\hbar\omega = 2\Delta$. Our calculation of 2D s -wave tight-binding model shows maximum of $\text{Im}[\sigma_{SHG,xxx}^{(2)}]$ is about $7.2 \times 10^{-13} \text{ m} \cdot (\Omega \cdot \text{V})^{-1}$, the 3D SHG conductivity can be obtained by 2D value multiplied by the measured Fermi wavevector of NbN $k_F \approx 1.45 \text{ \AA}^{-1}$ [28, 46]. Converted to susceptibility, the final result is $\chi_{th}^{(2)} \approx 3.9 \times 10^8$ pm/V, which matches well with the experimental result. Meanwhile, the current induced peak in $\text{Im}[\sigma^{(2)}(\omega)]$ is predicted to be proportional to square of the supercurrent density, which is also consistent with the experimental observations [32]. All of these mean that the proposed effect may have very well already been observed. However, more detailed studies are required to convincingly separate our mechanism from one based on vortex dynamics in that experiment.

So far we only consider a clean system, the effect of impurity scattering can be considered as a positive imaginary parameter into Green's function. Thus the resulting response from both linear- and second-order is reduced, especially near the resonance frequency region, and the divergent behavior in low-frequency limit is replaced by approaching to a large value. In the dirty limit, the linear response will return to Mattis-Bardeen theory [11], which is also similar in second-order effect, the optical response near gap edge will be reduced since a small supercurrent does not dramatically change band structure. Recently the second-order optical effect of diffusive superconductor has been studied [47].

In summary, we have studied a supercurrent enabled second-order optical response in BCS superconductors of the clean limit. Such a supercurrent flow can be induced and controlled by an external magnetic field through the Meissner effect. Similar to the linear order case, we find a large second-order response near the gap edge in the presence of dc supercurrent. After vertex correction, all the magnitude of the linear- and second-order responses are reduced, only some second-order components even reverse sign, while the shape of frequency dependence curve is unchanged. Here we point out that the contribution from collective modes have already been included in vertex correction reflecting the BCS electron-electron interactions. For the above several examples with typical superconducting order parameters, we show the current enabled second-order optical conductivity strongly depend on the type of superconducting pairing as well as the nature of normal state. As such, the supercurrent induced nonlinear optical spectroscopy provides a valuable toolbox to explore novel superconductors. Moreover, although we only present nonlinear response up to second order in this manuscript, the diagrammatic method with vertex correction can be readily extended to higher order optical response.

Note added: During the finalization of our manuscript, we learned of an independent work on the second-order optical Hall response of superconductors [48]. They con-

sider the case of weak disorder, which is different from our case.

ACKNOWLEDGMENTS

This work is supported by the National Key Research Program of China under Grant No. 2019YFA0308404, the Natural Science Foundation of China through Grant No. 12174066, Science and Technology Commission of Shanghai Municipality under Grant No. 20JC1415900, the Innovation Program for Quantum Science and Technology through Grant No. 2021ZD0302600, Shanghai Municipal Science and Technology Major Project under Grant No. 2019SHZDZX01.

Appendix A: Ward-Takahashi identity

Here we derive the Ward-Takahashi identity in superconducting system, and apply it into optical response to maintain the gauge invariance, which leads to vertex correction. The partition function is

$$Z = \int \mathcal{D}\bar{\Psi}\mathcal{D}\Psi e^{-S[\bar{\Psi},\Psi,A]}. \quad (\text{A1})$$

where S is the action for superconductor without electromagnetic field, $\Psi = (\psi_\uparrow, \psi_\downarrow)^T$ is the Nambu bi-spinor. The generating functional of connected Green's function is

$$G = \ln \int \mathcal{D}\bar{\Psi}\mathcal{D}\Psi e^{-S[\bar{\Psi},\Psi,A] - \int d\mathbf{r} (J_{A_\mu} A_\mu + J_{\bar{\Psi}} \Psi + J_\Psi \bar{\Psi})}, \quad (\text{A2})$$

where J_{A_μ} , $J_{\bar{\Psi}}$ and J_Ψ are auxiliary fields. The expectation value of A_μ , $\bar{\Psi}$ and Ψ can be calculated through generating functional:

$$\langle A_\mu \rangle = \partial_\mu \left(\frac{\delta G}{\delta J_{A_\mu}} \right), \langle \bar{\Psi} \rangle = \partial_\mu \left(\frac{\delta G}{\delta J_{\bar{\Psi}}} \right), \langle \Psi \rangle = \partial_\mu \left(\frac{\delta G}{\delta J_\Psi} \right). \quad (\text{A3})$$

The generating functional of irreducible vertex function is obtained via Legendre transformation: $\Gamma = G - \int d\mathbf{r} (\langle A_\mu \rangle J_{A_\mu} + \langle \bar{\Psi} \rangle J_{\bar{\Psi}} + \langle \Psi \rangle J_\Psi)$. Taking functional derivative of Γ will give vertex functions

$$J_{A_\mu} = \partial_\mu \left(\frac{\delta \Gamma}{\delta \langle A_\mu \rangle} \right), J_{\bar{\Psi}} = \partial_\mu \left(\frac{\delta \Gamma}{\delta \langle \bar{\Psi} \rangle} \right), J_\Psi = \partial_\mu \left(\frac{\delta \Gamma}{\delta \langle \Psi \rangle} \right). \quad (\text{A4})$$

Gauge invariance requires G is invariant under infinitesimal $U(1)$ transformation: $\Psi' = (\tau_0 + i\theta\tau_3)\Psi$, $\bar{\Psi}' = (\tau_0 - i\theta\tau_3)\bar{\Psi}$, $A'_\mu = A_\mu - \partial_\mu\theta$. From $\delta G/\delta\theta = 0$ we have:

$$\partial_\mu \left(\frac{\delta \Gamma}{\delta \langle A_\mu \rangle} \right) = i \left(\frac{\delta \Gamma}{\delta \langle \bar{\Psi} \rangle} \tau_3 \Psi - \bar{\Psi} \frac{\delta \Gamma}{\delta \langle \Psi \rangle} \right). \quad (\text{A5})$$

Series of Ward identities can be derived from Eq. (A5) by taking functional derivative of both sides with respect

to the expectation value of fields. For example, taking functional derivative with respect to $\langle \bar{\Psi} \rangle$ and $\langle \Psi \rangle$ gives

$$\partial_{x^\mu} \frac{\delta^3 \Gamma}{\delta \langle \bar{\Psi}(z) \rangle \delta \langle \Psi(y) \rangle \delta \langle A_\mu(x) \rangle} = i \left[\frac{\delta^2 \Gamma}{\delta \langle \bar{\Psi}(z) \rangle \delta \langle \Psi(x) \rangle} \times \tau_3 \delta(x-y) - \tau_3 \frac{\delta^2 \Gamma}{\delta \langle \bar{\Psi}(x) \rangle \delta \langle \Psi(y) \rangle} \delta(x-z) \right]. \quad (\text{A6})$$

Converted to momentum representation, Eq. (A6) becomes Ward-Takahashi identity: $q_\mu \Gamma_\mu^1(k+q, k) = \tau_3 G^{-1}(k) - G^{-1}(k+q) \tau_3$, which gives the connection between Green's function and one-photon vertex function. The relation between self-energy correction term $\Sigma(k)$ and one-photon vertex correction term $\Lambda_\mu^1(k+q, k)$ can directly obtained by Ward-Takahashi identity

$$q_\mu \Lambda_\mu^1(k+q, k) = \Sigma(k+q) \tau_3 - \tau_3 \Sigma(k). \quad (\text{A7})$$

In addition, if we further take functional derivative of Eq. (A6) with respect to $\langle A_\mu \rangle$, we will get the relation between one-photon vertex correction term $\Lambda_\mu^1(k+q, k)$ and two-photon vertex correction term $\Lambda_{\mu,\nu}^2(k+q'+q, k)$:

$$q_\mu \Lambda_{\mu,\nu}^2(k+q'+q, k) = \Lambda_\mu^1(k+q'+q, k) \tau_3 - \tau_3 \Lambda_\mu^1(k+q', k) \quad (\text{A8})$$

Similar procedure can be done to get relation between n -photon vertex correction term and $n+1$ -photon vertex correction term:

$$q_\mu \Lambda_{\mu,\nu}^{n+1}(k+q'+q, k) = \Lambda_\mu^n(k+q'+q, k) \tau_3 - \tau_3 \Lambda_\mu^n(k+q', k) \quad (\text{A9})$$

Diagrammatical description is shown in Fig. 13, which needs to be satisfied when calculating higher order optical response of superconductor. In this sense, self-energy correction term $\Sigma(k)$ can be viewed as zero-photon vertex correction term $\Lambda^0(k)$.

Appendix B: Vertex correction for optical response

Here we give the detailed calculation of vertex correction in the single-band superconductor models, then apply to optical response.

The $\gamma_{a_1, a_2, \dots, a_n}$ matrix can be decomposed into two components in terms of Pauli matrices: $\gamma_{a_1, a_2, \dots, a_n} = \gamma_{a_1, a_2, \dots, a_n}^{(1)} \tau_0 + \gamma_{a_1, a_2, \dots, a_n}^{(2)} \tau_3$. Similarly, the corrected vertex, Γ matrix can be expanded as,

$$\Gamma_{a_1, a_2, \dots, a_n} = \gamma_{a_1, a_2, \dots, a_n} + \sum_{i=0}^3 \Gamma_{a_1, a_2, \dots, a_n}^{(i)} \tau_i. \quad (\text{B1})$$

In s -wave case, $\Gamma(p+q, p)$ is independent of p , and photon momentum \mathbf{q} is negligible, thus all expansion coefficients of Γ matrix can be solved by self-consistent equation Eq. (7) at every frequency of incident light.

To find out resonance frequency clearly, we sum over the imaginary temporal component and re-express the

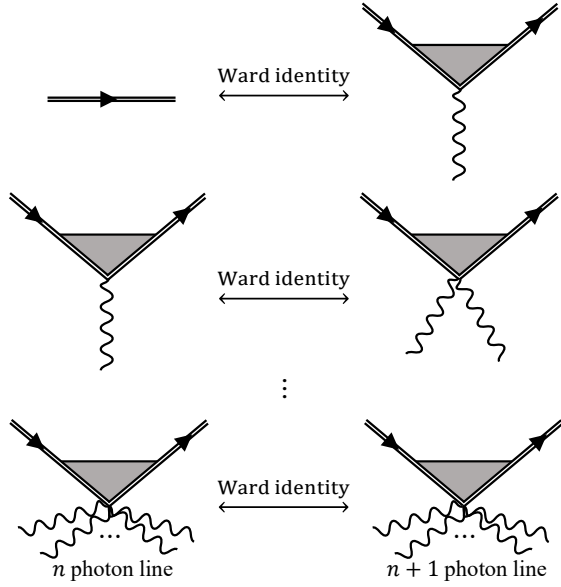


FIG. 13. Diagrammatical description of Ward identities. The n -photon vertex correction term has quantitative relation to $n + 1$ -photon vertex correction term.

formulas of $\sigma^{(1)}$ and $\sigma^{(2)}$. The diagram in Fig. 3(a) gives,

$$\int [d\mathbf{k}] \left(-\gamma_{ab}^{(1)} + \frac{\bar{\epsilon}_{\mathbf{k}} \gamma_{ab}^{(2)}}{E'_{\mathbf{k}}} \right), \quad (\text{B2})$$

where we denote $\bar{\epsilon}_{\mathbf{k}} = (\epsilon_{\mathbf{k}+\mathbf{q}} + \epsilon_{-\mathbf{k}+\mathbf{q}})/2$, $E'_{\mathbf{k}} = \sqrt{\bar{\epsilon}_{\mathbf{k}}^2 + \Delta^2}$ and abbreviate the integral over \mathbf{k} to $\int [d\mathbf{k}]$. Fig. 3(b) gives

$$\int [d\mathbf{k}] \frac{2\Delta}{E'_{\mathbf{k}} [4E_{\mathbf{k}}'^2 - (\hbar\tilde{\omega})^2]} \left[-2\bar{\epsilon}_{\mathbf{k}} \Gamma_b^{(1)}(\omega) \gamma_a^{(2)} + i\hbar\tilde{\omega} \Gamma_b^{(2)}(\omega) \gamma_a^{(2)} + 2\Delta(\gamma_a^{(2)} \gamma_b^{(2)} + \Gamma_b^{(3)}(\omega) \gamma_a^{(2)}) \right] \quad (\text{B3})$$

where $\tilde{\omega} = \omega + i0^+$. The denominator indicates that the resonance frequency is $\hbar\omega \approx 2\Delta$. Eq. (10) consists of four parts, each is represented by a diagram in Fig. 3(e)-3(f). The first part reads

$$\int [d\mathbf{k}] \left(\gamma_{abc}^{(1)} + \frac{\bar{\epsilon}_{\mathbf{k}} \gamma_{abc}^{(2)}}{E'_{\mathbf{k}}} \right). \quad (\text{B4})$$

The second part is a bubble diagram

$$\int [d\mathbf{k}] \frac{-2\Delta}{E'_{\mathbf{k}} [4E_{\mathbf{k}}'^2 - (\hbar\tilde{\omega}_2)^2]} \left[-2\bar{\epsilon}_{\mathbf{k}} \Gamma_c^{(1)}(\omega_2) \gamma_{ab}^{(2)} + i\hbar\tilde{\omega}_2 \Gamma_c^{(2)}(\omega_2) \gamma_{ab}^{(2)} + 2\Delta(\gamma_{ab}^{(2)} \gamma_c^{(2)} + \Gamma_c^{(3)}(\omega_2) \gamma_{ab}^{(2)}) \right] + (b, \omega_1) \leftrightarrow (c, \omega_2) \quad (\text{B5})$$

The denominator indicates that the resonance frequency

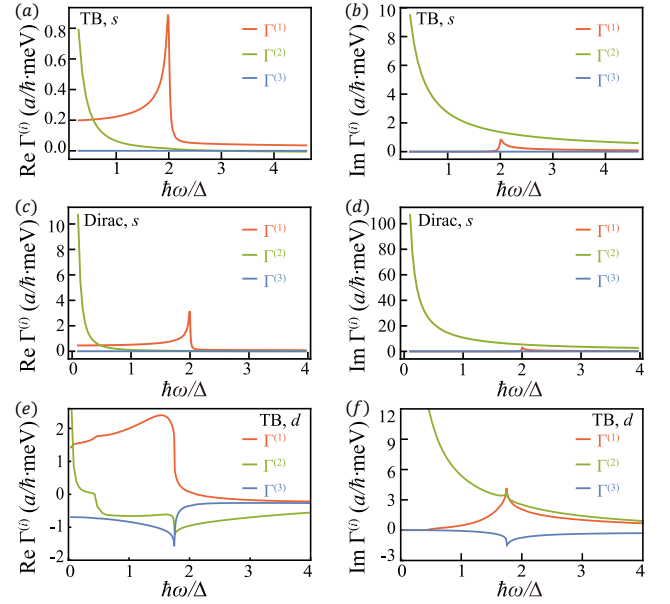


FIG. 14. Components of Γ vs. frequency. (a) and (b) are calculated from s -wave tight-binding model, (c) and (d) are calculated from Dirac fermion model, (e) and (f) are calculated from d -wave tight-binding model.

is $\hbar\omega \approx 2\Delta$. The third part is another bubble diagram

$$\int [d\mathbf{k}] \frac{-2\Delta}{E'_{\mathbf{k}} [4E_{\mathbf{k}}'^2 - (\hbar\tilde{\omega}_{12})^2]} \left[-2\bar{\epsilon}_{\mathbf{k}} \Gamma_c^{(1)}(-\omega_{12}) \gamma_{bc}^{(2)} - i\hbar\tilde{\omega}_{12} \Gamma_c^{(2)}(-\omega_{12}) \gamma_{bc}^{(2)} + 2\Delta(\gamma_{bc}^{(2)} \gamma_a^{(2)} + \Gamma_c^{(3)}(-\omega_{12}) \gamma_{bc}^{(2)}) \right] \quad (\text{B6})$$

Where $\omega_{12} = \omega_1 + \omega_2$ and $\tilde{\omega}_{12} = \tilde{\omega}_1 + \tilde{\omega}_2$. The denominator indicates that in the case of SHG, the resonance frequency is $\hbar\omega \approx \Delta$, and in the case of photocurrent effect, no resonance frequency appears.

The triangular diagram is far more complicated, we only show the result without vertex correction,

$$\int [d\mathbf{k}] \frac{16\Delta^2 \bar{\epsilon}_{\mathbf{k}} [12E_{\mathbf{k}}'^2 - (\hbar\tilde{\omega}_{12})^2 + \hbar\tilde{\omega}_1 \hbar\tilde{\omega}_2] \gamma_a^{(2)} \gamma_b^{(2)} \gamma_c^{(2)}}{E'_{\mathbf{k}} [4E_{\mathbf{k}}'^2 - (\hbar\tilde{\omega}_{12})^2] [4E_{\mathbf{k}}'^2 - (\hbar\tilde{\omega}_1)^2] (4E_{\mathbf{k}}'^2 - (\hbar\tilde{\omega}_2)^2)} \quad (\text{B7})$$

Likewise, denominator indicates that for SHG, the resonance frequencies are $\hbar\omega \approx \Delta$ and $\hbar\omega \approx 2\Delta$, for photocurrent effect, resonance frequency is $\hbar\omega \approx 2\Delta$. Vertex correction will modify this term significantly, while leaving the resonance frequencies unchanged, which can be seen in the Dirac fermion case in the main text.

As a side note, if there is no supercurrent, $q = 0$, $\gamma_a^{(2)} = \gamma_{ab}^{(1)} = \gamma_{abc}^{(2)} = 0$, thus Eq. (B3)-(B6) and the real part of Eq. (B2) vanish in the condition of $\epsilon_{\mathbf{k}} = \epsilon_{-\mathbf{k}}$. Only imaginary part of $\sigma^{(1)}$ survives and no optical transition at any finite frequency, verifying the effect of supercurrent. Besides, the zero response of second order reflects inversion symmetry of the system when $q = 0$.

In the d -wave case, $V_{\mathbf{k}, \mathbf{k}'}$ can factorized as: $V \phi_{\mathbf{k}} \phi_{\mathbf{k}'}$, where V is a constant and $\phi_{\mathbf{k}} = (\cos k_x - \cos k_y)$, the

self-consistent equation for corrected vertex function becomes:

$$\frac{\Gamma(p+q, p)}{\phi_{\mathbf{p}}} = \frac{\gamma(p+q, p)}{\phi_{\mathbf{p}}} + V \frac{1}{\beta} \sum_{k_0} \int \frac{d^2 \mathbf{k}}{(2\pi)^2} \quad (\text{B8})$$

$$[\phi_{\mathbf{k}} \tau_3 G(k_0 + q_0, \mathbf{k} + \mathbf{q}) \Gamma(k+q, k) G(k_0, \mathbf{k}) \tau_3]$$

After divided by $\phi_{\mathbf{p}}$, the integrand above is independent of \mathbf{p} , thus we can expand Γ matrix as:

$$\Gamma(p+q, p) = \gamma(p+q, p) + \phi_{\mathbf{p}} \sum_{i=0}^3 \Gamma^{(i)} \tau_i \quad (\text{B9})$$

In this manner, all expansion coefficients of Γ matrix can be solved through Eq. (B8) for every frequency (again, we consider $\mathbf{q} = 0$), then the optical responses of d -wave superconductor can be obtained by Eq. (9) and (10).

We show $\Gamma^{(1)}, \Gamma^{(2)}, \Gamma^{(3)}$ with respect to frequency calculated from s -wave tight-binding model, Dirac fermion model and d -wave tight-binding model in Fig. 14.

Clearly, in the first two models, $\Gamma^{(1)}$ has a peak near resonance frequency, while $\Gamma^{(2)}$ is almost proportional to ω^{-1} , and $\Gamma^{(3)}$ can be neglected compared with $\Gamma^{(1)}$ and $\Gamma^{(2)}$. We found that the $\Gamma^{(1)}$ components contributes little to modification of bubble diagram but is important to modification of triangular diagram, thus can change the second order conductivity distinctly in Dirac fermion model. In d -wave case, besides the peaks near $\hbar\omega = 2\Delta$ and ω^{-1} divergence of $\Gamma^{(2)}$ at low frequency region, more complex behaviors appear, especially near the frequency region when optical transition occurs near Bogoliubov Fermi surface that induced by supercurrent. These behaviors are reflected in the intricate response after vertex correction of d -wave superconductor.

Appendix C: Analytical result for optical responses of Dirac fermion with s -wave pairing

The optical conductivity for Dirac fermion with s -wave superconducting pairing without vertex correction can be calculated analytically. The real part of $\sigma_{xx}^{(1)}$ is

$$\text{Re}(\sigma^{(1)}(\omega)) = \frac{e^2}{\hbar} 3\pi^2 \frac{\Delta}{\mu} \frac{(\hbar v q)^2}{(\hbar\omega)^2} \frac{\Delta}{\sqrt{(\hbar\omega)^2 - 4\Delta^2}} \Theta[\hbar\omega - 2\Delta] \quad (\text{C1})$$

and imaginary part can be obtain via Kramers-Kronig (K-K) relation as

$$\text{Im}(\sigma^{(1)}(\omega)) = \frac{e^2}{\hbar} 6\pi \frac{\Delta}{\mu} \frac{(\hbar v q)^2}{(\hbar\omega)^2} \begin{cases} -\frac{\Delta \arcsin(\frac{\hbar\omega}{2\Delta})}{\sqrt{4\Delta^2 - (\hbar\omega)^2}} & 0 < \hbar\omega < 2\Delta \\ \frac{\Delta \text{arcosh}(\frac{\hbar\omega}{2\Delta})}{\sqrt{(\hbar\omega)^2 - 4\Delta^2}} & \hbar\omega > 2\Delta \end{cases} \quad (\text{C2})$$

$\sigma_{yy}^{(1)}(\omega) = \sigma_{xx}^{(1)}(\omega)/3$ due to the difference between γ_x and γ_y in angular integrations.

The imaginary part of $\sigma_{\text{SHG},xxx}^{(2)}(\omega)$ is:

$$\text{Im}[\sigma_{\text{SHG},xxx}^{(2)}(\omega)] = -\frac{e^3}{\hbar^2} 5\pi^2 \frac{\Delta^2}{\mu^2} \frac{(\hbar v q)^3}{(\hbar\omega)^5} \frac{\hbar v}{\mu} \left(\sqrt{(\hbar\omega)^2 - \Delta^2} \Theta[\hbar\omega - \Delta] - \sqrt{(\hbar\omega)^2 - 4\Delta^2} \Theta[\hbar\omega - 2\Delta] \right) \quad (\text{C3})$$

Through generalized K-K relation for nonlinear response [49], the real part is given by:

$$\text{Re}[\sigma_{\text{SHG},xxx}^{(2)}(\omega)] = \frac{e^3}{\hbar} 10\pi \frac{\Delta^2}{\mu^2} \frac{(\hbar v q)^3}{(\hbar\omega)^5} \frac{\hbar v}{\mu} \begin{cases} \sqrt{\Delta^2 - (\hbar\omega)^2} \arcsin(\frac{\hbar\omega}{\Delta}) - \sqrt{4\Delta^2 - (\hbar\omega)^2} \arcsin(\frac{\hbar\omega}{2\Delta}) & 0 < \hbar\omega < \Delta \\ \sqrt{(\hbar\omega)^2 - \Delta^2} \text{arcosh}(\frac{\hbar\omega}{\Delta}) - \sqrt{4\Delta^2 - (\hbar\omega)^2} \arcsin(\frac{\hbar\omega}{2\Delta}) & \Delta < \hbar\omega < 2\Delta \\ \sqrt{(\hbar\omega)^2 - \Delta^2} \text{arcosh}(\frac{\hbar\omega}{\Delta}) - \sqrt{(\hbar\omega)^2 - 4\Delta^2} \text{arcosh}(\frac{\hbar\omega}{2\Delta}) & \hbar\omega > 2\Delta \end{cases} \quad (\text{C4})$$

$\sigma_{\text{PC},xxx}^{(2)}(\omega)$ is purely real:

$$\sigma_{\text{PC},xxx}^{(2)}(\omega) = \frac{e^3}{\hbar} \frac{5\pi}{2} \frac{\Delta^2}{\mu^2} \frac{(\hbar v q)^3}{(\hbar\omega)^3} \frac{\hbar v}{\mu} \left(\frac{\hbar\omega}{\Delta^2} + \frac{1}{\eta} \frac{2\pi \sqrt{(\hbar\omega)^2 - 4\Delta^2} \Theta[\hbar\omega - 2\Delta]}{\hbar\omega} \right) \quad (\text{C5})$$

where η is a small positive parameter, which is set to be 5×10^{-2} meV in the calculation of main text. Sim-

ilarly, the different factor of angular integral for γ_x and γ_y results in $\sigma_{xy}^{(2)} = \sigma_{yy}^{(2)} = \sigma_{xx}^{(2)}/5$.

[1] Joseph Orenstein, "Ultrafast spectroscopy of quantum materials," *Phys. Today* **65**, 44–50 (2012).

[2] D. N. Basov, Richard D. Averitt, Dirk van der Marel,

- Martin Dressel, and Kristjan Haule, “Electrodynamics of correlated electron materials,” *Rev. Mod. Phys.* **83**, 471–541 (2011).
- [3] M. Tinkham, “The electromagnetic properties of superconductors,” *Rev. Mod. Phys.* **46**, 587–596 (1974).
 - [4] D. N. Basov and T. Timusk, “Electrodynamics of high- T_c superconductors,” *Rev. Mod. Phys.* **77**, 721–779 (2005).
 - [5] Jing Wang, Bang-Fen Zhu, and Ren-Bao Liu, “Second-order nonlinear optical effects of spin currents,” *Phys. Rev. Lett.* **104**, 256601 (2010).
 - [6] Lalani K. Werake and Hui Zhao, “Observation of second-harmonic generation induced by pure spin currents,” *Nature Phys.* **6**, 875–878 (2010).
 - [7] Jing Wang, Bang-Fen Zhu, and Ren-Bao Liu, “Proposal for direct measurement of a pure spin current by a polarized light beam,” *Phys. Rev. Lett.* **100**, 086603 (2008).
 - [8] H. J. A. Molegraaf, C. Presura, D. van der Marel, P. H. Kes, and M. Li, “Superconductivity-induced transfer of in-plane spectral weight in $\text{Bi}_2\text{Sr}_2\text{CaCu}_2\text{O}_{8+\delta}$,” *Science* **295**, 2239–2241 (2002).
 - [9] L. Degiorgi, G. Briceno, M. S. Fuhrer, A. Zettl, and P. Wachter, “Optical measurements of the superconducting gap in single-crystal K_3C_{60} and Rb_3C_{60} ,” *Nature* **369**, 541–543 (1994).
 - [10] A. V. Pronin, M. Dressel, A. Pimenov, A. Loidl, I. V. Roshchin, and L. H. Greene, “Direct observation of the superconducting energy gap developing in the conductivity spectra of niobium,” *Phys. Rev. B* **57**, 14416–14421 (1998).
 - [11] D. C. Mattis and J. Bardeen, “Theory of the anomalous skin effect in normal and superconducting metals,” *Phys. Rev.* **111**, 412–417 (1958).
 - [12] Gerald D. Mahan, *Many-Particle Physics* (Springer US, Boston, MA, 2000).
 - [13] W. Zimmermann, E.H. Brandt, M. Bauer, E. Seider, and L. Genzel, “Optical conductivity of bcs superconductors with arbitrary purity,” *Physica C* **183**, 99–104 (1991).
 - [14] Junyeong Ahn and Naoto Nagaosa, “Theory of optical responses in clean multi-band superconductors,” *Nature Commun.* **12**, 1617 (2021).
 - [15] Tianrui Xu, Takahiro Morimoto, and Joel E. Moore, “Nonlinear optical effects in inversion-symmetry-breaking superconductors,” *Phys. Rev. B* **100**, 220501 (2019).
 - [16] Hikaru Watanabe, Akito Daido, and Youichi Yanase, “Nonreciprocal optical response in parity-breaking superconductors,” *Phys. Rev. B* **105**, 024308 (2022).
 - [17] Hiroto Tanaka, Hikaru Watanabe, and Youichi Yanase, “Nonlinear optical responses in noncentrosymmetric superconductors,” *Phys. Rev. B* **107**, 024513 (2023).
 - [18] T. Cea, C. Castellani, and L. Benfatto, “Nonlinear optical effects and third-harmonic generation in superconductors: Cooper pairs versus higgs mode contribution,” *Phys. Rev. B* **93**, 180507 (2016).
 - [19] Naoto Tsuji, Yuta Murakami, and Hideo Aoki, “Nonlinear light-higgs coupling in superconductors beyond bcs: Effects of the retarded phonon-mediated interaction,” *Phys. Rev. B* **94**, 224519 (2016).
 - [20] Ryusuke Matsunaga, Naoto Tsuji, Kazumasa Makise, Hirotaka Terai, Hideo Aoki, and Ryo Shimano, “Polarization-resolved terahertz third-harmonic generation in a single-crystal superconductor nbn: Dominance of the higgs mode beyond the bcs approximation,” *Phys. Rev. B* **96**, 020505 (2017).
 - [21] T. Cea, P. Barone, C. Castellani, and L. Benfatto, “Polarization dependence of the third-harmonic generation in multiband superconductors,” *Phys. Rev. B* **97**, 094516 (2018).
 - [22] F. Yang and M. W. Wu, “Gauge-invariant microscopic kinetic theory of superconductivity in response to electromagnetic fields,” *Phys. Rev. B* **98**, 094507 (2018).
 - [23] F. Yang and M. W. Wu, “Gauge-invariant microscopic kinetic theory of superconductivity: Application to the optical response of nambu-goldstone and higgs modes,” *Phys. Rev. B* **100**, 104513 (2019).
 - [24] Ryusuke Matsunaga, Naoto Tsuji, Hiroyuki Fujita, Arata Sugioka, Kazumasa Makise, Yoshinori Uzawa, Hirotaka Terai, Zhen Wang, Hideo Aoki, and Ryo Shimano, “Light-induced collective pseudospin precession resonating with higgs mode in a superconductor,” *Science* **345**, 1145–1149 (2014).
 - [25] Andreas Moor, Anatoly F. Volkov, and Konstantin B. Efetov, “Amplitude higgs mode and admittance in superconductors with a moving condensate,” *Phys. Rev. Lett.* **118**, 047001 (2017).
 - [26] Matteo Puviani, Lukas Schwarz, Xiao-Xiao Zhang, Stefan Kaiser, and Dirk Manske, “Current-assisted raman activation of the higgs mode in superconductors,” *Phys. Rev. B* **101**, 220507 (2020).
 - [27] Philip J. D. Crowley and Liang Fu, “Supercurrent-induced resonant optical response,” *Phys. Rev. B* **106**, 214526 (2022).
 - [28] Michał Papaj and Joel E. Moore, “Current-enabled optical conductivity of superconductors,” *Phys. Rev. B* **106**, L220504 (2022).
 - [29] X. Yang, C. Vaswani, C. Sundahl, M. Mootz, L. Luo, J. H. Kang, I. E. Perakis, C. B. Eom, and J. Wang, “Lightwave-driven gapless superconductivity and forbidden quantum beats by terahertz symmetry breaking,” *Nature Photonics* **13**, 707–713 (2019).
 - [30] C. Vaswani, M. Mootz, C. Sundahl, D. H. Mudiyanse-lage, J. H. Kang, X. Yang, D. Cheng, C. Huang, R. H. J. Kim, Z. Liu, L. Luo, I. E. Perakis, C. B. Eom, and J. Wang, “Terahertz second-harmonic generation from lightwave acceleration of symmetry-breaking nonlinear supercurrents,” *Phys. Rev. Lett.* **124**, 207003 (2020).
 - [31] Sachiko Nakamura, Yudai Iida, Yuta Murotani, Ryusuke Matsunaga, Hirotaka Terai, and Ryo Shimano, “Infrared activation of the higgs mode by supercurrent injection in superconducting nbn,” *Phys. Rev. Lett.* **122**, 257001 (2019).
 - [32] Sachiko Nakamura, Kota Katsumi, Hirotaka Terai, and Ryo Shimano, “Nonreciprocal terahertz second-harmonic generation in superconducting nbn under supercurrent injection,” *Phys. Rev. Lett.* **125**, 097004 (2020).
 - [33] J. Bardeen, “Gauge invariance and the energy gap model of superconductivity,” *Il Nuovo Cimento* **5**, 1766–1768 (1957).
 - [34] J. Robert Schrieffer, *Theory of Superconductivity* (CRC Press, Boca Raton, 1999).
 - [35] Yoichiro Nambu, “Quasi-particles and gauge invariance in the theory of superconductivity,” *Phys. Rev.* **117**, 648–663 (1960).
 - [36] Zhehao Dai and Patrick A. Lee, “Optical conductivity from pair density waves,” *Phys. Rev. B* **95**, 014506 (2017).
 - [37] Nikolai Nikolaevich Bogolyubov, “The compensation principle and the self-consistent field method,” *Sov. Phys.*

- Usp.* **2**, 236 (1959).
- [38] Piers Coleman, *Introduction to Many-Body Physics*, 2nd ed. (Cambridge University Press, 2015).
 - [39] Chang geun Oh and Haruki Watanabe, “Electromagnetic response of superconductors in mean-field approximation,” (2023), [arXiv:2304.07432 \[cond-mat.supr-con\]](#).
 - [40] Daniel E. Parker, Takahiro Morimoto, Joseph Orenstein, and Joel E. Moore, “Diagrammatic approach to nonlinear optical response with application to weyl semimetals,” *Phys. Rev. B* **99**, 045121 (2019).
 - [41] Yoshihiro Michishita and Robert Peters, “Effects of renormalization and non-hermiticity on nonlinear responses in strongly correlated electron systems,” *Phys. Rev. B* **103**, 195133 (2021).
 - [42] Habib Rostami and Emmanuele Cappelluti, “Dominant role of two-photon vertex in nonlinear response in two-dimensional dirac systems,” *npj 2D Mater. Appl* **5**, 50 (2021).
 - [43] Hikaru Watanabe, Akito Daido, and Youichi Yanase, “Nonreciprocal meissner response in parity-mixed superconductors,” *Phys. Rev. B* **105**, L100504 (2022).
 - [44] Zhen Zhu, Michał Papaj, Xiao-Ang Nie, Hao-Ke Xu, Yi-Sheng Gu, Xu Yang, Dandan Guan, Shiyong Wang, Yaoyi Li, Canhua Liu, Jianlin Luo, Zhu-An Xu, Hao Zheng, Liang Fu, and Jin-Feng Jia, “Discovery of segmented fermi surface induced by cooper pair momentum,” *Science* **374**, 1381–1385 (2021).
 - [45] D. J. Passos, G. B. Ventura, J. M. Viana Parente Lopes, J. M. B. Lopes Dos Santos, and N. M. R. Peres, “Nonlinear optical responses of crystalline systems: Results from a velocity gauge analysis,” *Phys. Rev. B* **97**, 235446 (2018).
 - [46] S. P. Chockalingam, Madhavi Chand, John Jesudasan, Vikram Tripathi, and Pratap Raychaudhuri, “Superconducting properties and hall effect of epitaxial nbn thin films,” *Phys. Rev. B* **77**, 214503 (2008).
 - [47] Pascal Derendorf, Anatoly F. Volkov, and Ilya M. Eremin, “Nonlinear response of diffusive superconductors to *ac*-electromagnetic fields,” (2023), [arXiv:2308.00838 \[cond-mat.supr-con\]](#).
 - [48] A. V. Parafilo, V. M. Kovalev, and I. G. Savenko, “Photoinduced anomalous supercurrent hall effect,” (2023), [arXiv:2307.03314 \[cond-mat.supr-con\]](#).
 - [49] F. Bassani and S. Scandolo, “Sum rules for nonlinear optical susceptibilities,” *Phys. Status Solidi* **173**, 263–270 (1992).